Funneling of Flow into Grain-to-grain Contacts Drives Colloid−Colloid Aggregation in the Presence of an Energy Barrier

MEIPING TONG,[†] HUILIAN MA, AND WILLIAM P. JOHNSON*

Department of Geology and Geophysics, University of Utah, Salt Lake City, Utah 84112

Deposition behaviors of carboxylate-modified polystyrene latex microspheres (five sizes ranging from 0.1 to 2.0 μm) were examined in packed porous media, impinging jet, and porous media-packed flow chamber systems under a variety of environmentally relevant ionic strength and flow conditions in the presence of an energy barrier to deposition. Temporally constant deposition rate coefficients were observed for all microsphere sizes under baseline conditions, whereas temporal increases in colloid deposition rate coefficients (ripening) occurred for all microsphere sizes in response to slight increases in solution ionic strength and slight decreases in fluid velocity. This transition from "clean bed" deposition to ripening was triggered by relatively subtle changes in solution chemistry and fluid velocity. Direct observation of colloid deposition in a flow chamber packed with porous media revealed that colloidal aggregates formed at grain-to-grain contacts in the porous media. The absence of ripening in an impinging jet system (unbounded flat surface) examined under equivalent conditions to the packed porous media further indicated that colloid aggregation was driven by the funneling of fluid into the grain-to-grain contacts. Comparison of colloid breakthrough in porous media comprised of smooth-spherical versus angular grains demonstrated that the propensity to trigger ripening increased with the number and length of grain-to-grain contacts.

Introduction

Temporal increases in colloid deposition rate coefficients in porous media may occur due to colloid attachment to previously deposited colloids, a process called filter ripening (e.g., refs *1−7*). Two decades ago, O'Melia and Ali (*1*) found that the head-loss in their systems was related to colloid aggregation (ripening) and developed a classic filter-ripening model to explain the observed head-loss and the extra removal of colloids by previously deposited particles. Their work inspired subsequent work in the development of filter-ripening models (e.g., refs *7−10*), and filter ripening was reported to occur under particular solution chemistry conditions (e.g., refs *4−6*). Existing work regarding filter ripening has not specified the location of colloid−colloid aggregation

in the pore domain, and the conditions required for transition from "clean bed" conditions to ripening have not been well-examined. Bradford et al. (*11*) recently reported aggregation of colloids (*Escherichia coli* O157:H7) at grain-to-grain contacts in quartz sand under highly unfavorable conditions (pure water). The authors suggested that funneling of flow into grain-to-grain contacts might account for the aggregation of colloids under this highly unfavorable condition.

The objective of this paper is to examine the transition from "clean bed" conditions (under which the colloid deposition rate coefficient is temporally constant) to conditions where ripening occurs (temporally increased deposition rate coefficient). We demonstrate that subtle changes in solution chemistry and fluid velocity can trigger transition from "clean bed" deposition to ripening. More important, we provide experimental observations to support the hypothesis that funneling of fluid into grain-to-grain contacts drives the observed aggregation of colloids in porous media and that the propensity for filter ripening increases with the number and length of grain-to-grain contacts.

Materials and Methods

Microspheres. Spherical fluorescent carboxylate-modified polystyrene latex microspheres (Molecular Probes, Inc., Eugene, Oregon) of five sizes (diameters of 0.1, 0.2, 0.5, 1.0, and 2.0 μm, with negative surface charge densities of 0.3207, 0.282, 0.1419, 0.0175, and 0.1076 meq g^{-1}, respectively) were used in all experiments. The 0.1, 0.2, 0.5, 1.0, and 2.0 μm microsphere stock suspensions had particle concentrations of 3.6×10^{13}, 4.5×10^{12}, 2.9×10^{11}, 2.7×10^{10}, and 4.5×10^{9} microspheres mL^{-1}, respectively. The stock solutions contained NaN$_3$ (2 mM); whereas the 2.0 μm microsphere stock suspension also included 0.01% Tween-20.

Prior to injection, stock solutions for the 0.1, 0.2, 0.5, and 1.0 μm microspheres were diluted in NaCl solution to achieve a nominal influent concentration (C_o) of $1.0 \times 10^{7} \pm 30\%$ particles mL^{-1} at the desired ionic strength (NaCl), plus MOPS buffer (2.2 mM), yielding a solution pH of 6.72. The stock solution for the 2.0 μm microspheres was first diluted 10 times in pure (Milli-Q) water (Millipore Corp. Bedford, Massachusetts) and was then washed three times to remove Tween-20. Washing involved centrifugation (10 000g for 10 min at 4 °C), followed by decanting and addition of pure water. Following washing, the 2.0 μm microsphere solution was diluted in NaCl solution to achieve a nominal influent concentration (C_o) of $1.0 \times 10^{6} \pm 30\%$ at the desired ionic strength (NaCl) plus MOPS buffer (2.2 mM), yielding a solution pH of 6.72. Experiments were conducted both at ionic strengths of 0.02 and 0.05 M for all microsphere sizes.

Porous Media Experiments. *Porous Media.* Spherical soda lime glass beads (Cataphote Inc. Jackson, Mississippi) and quartz sand (Unimin Corp., New Canaan, Connecticut) with sizes ranging from 417 to 600 μm (with median diameter of 510 μm) were used for microsphere deposition experiments in porous media. The procedure used for cleaning the glass beads and quartz sand is provided in previous publications (*12–14*).

Porous Media Experimental Conditions. Cylindrical Plexiglass columns (20 cm long, 3.81 cm inner diameter) were dry-packed with glass beads or quartz sand, flushed with CO$_2$, and pre-equilibrated with microsphere-free solution. The procedure of packing and pre-equilibration was described in previous publications (*12–14*). After pre-equilibration, a solution with microspheres was injected (3 pore volumes). This was followed by elution with microsphere-free solution (7 pore volumes).

* Corresponding author e-mail: wjohnson@mines.utah.edu, phone: (801) 581-5033, fax: (801) 581-7065.
† Current address: College of Environmental Sciences and Engineering, Peking University, the Key Laboratory of Water and Sediment Sciences, Ministry of Education, Beijing 100871, P. R. China.

diameter (µm)	porous media	ionic strength (M)	ave. pore water velocity (m day⁻¹)	mass recovery %	breakthrough %
0.1	glass beads	0.02	8	101.1	98.9
		0.05	8	106.8	87.5
	quartz sand	0.05	8	102.3	6.62
0.2	glass beads	0.02	8	105.2	90.6
		0.05	8	108.0	72.6
	quartz sand	0.05	8	88.7	0.8
0.5	glass beads	0.02	8	100.0	97.8
		0.05	8	101.7	90.2
			2	84.4	38.7
	quartz sand	0.05	8	99.6	0.11
1.0	glass beads	0.02	8	100.1	92.2
		0.05	8	92.7	66.1
			2	90.6	52.3
	quartz sand	0.05	8	89.4	2.6
2.0	glass beads	0.02	8	98.0	93.0
		0.05	8	92.7	66.4
			2	80.6	48.7
	quartz sand	0.05	8	98.8	8.5

[a] "Mass recovery %" refers to percent recovery of injected microspheres via effluent and via desorption following dissection. "Breakthrough %" refers to percent recovery of injected microspheres via breakthrough effluent.

During injection, the microsphere suspension reservoirs were sonicated for 1 min per hour to minimize aggregation, as verified by flow cytometric analyses. The flow rate was varied between experiments to produce pore water velocities at 2 and 8 m day⁻¹. The suspensions and solutions were injected in up-flow mode using a syringe pump (Harvard Apparatus, Inc., Holliston, Massachusetts).

Sample Collection and Analysis. Column effluent samples were collected in 5 mL polystyrene tubes using a fraction collector (CF-1, Spectrum Chromatography, Houston, Texas). Following the experiment, the sediment was dissected into 10 2 cm-long segments, as the sediment was released from the column under gravity. Retained colloids were recovered by placing sediment segments (2 cm) into specified volumes of Milli-Q water and sonicating for 1 min, followed by manual vigorous shaking for 30 s. Aqueous effluent samples, and supernatant samples from recovery of retained microspheres, were analyzed using flow cytometry (BD FACScan, Becton Dickinson and Co., Franklin Lakes, New Jersey); The samples were run using a flow rate of 12 µL-min⁻¹ at an excitation wavelength of 488 nm and were counted for 1 min. Conversion of "event" counts on the flow cytometer into microsphere concentrations was made using a calibration curve based on serial dilutions of microsphere suspensions of known concentration. The values of R^2 from the log–log calibration curves were consistently greater than 0.99. The flow cytometer was able to track aggregation of microspheres as doublets and triplets based on their respective light scattering properties. The area under the breakthrough-elution curve was integrated to yield the percentage of microspheres exiting the column. The percentage of injected microspheres recovered from the sediment was determined by summing the number of microspheres recovered from all segments of the sediment and then dividing by the total number injected. The overall recovery (mass balance) of microspheres was determined by summing the percentages of microspheres that exited and that were retained in the column. Mass recoveries (total from effluent and sediment) were virtually all between 81 and 108%, with the vast majority showing between 85 and 105% recovery (Table 1). The excellent mass balance shows that the microspheres were detached by dilution into pure water, indicating that their mechanism of attachment was eliminated either by disassembling the pore structure or by increasing the magnitude of colloid−collector electrostatic repulsion.

Impinging Jet Experiments. *Substrata Preparation.* Glass microscope slides (Fisher Scientific, Inc.) of dimension 25 × 75 × 1 mm were used in the impinging jet flow cell (15, 16). The procedure used for cleaning the glass slides was provided in previous publications (15, 16).

Impinging Jet Experimental Conditions. Colloid deposition experiments were performed in an impinging jet system (radial stagnation point flow) for the range of microsphere sizes, fluid velocities, and solution chemistry conditions utilized in porous media experiments. The duration of experiments ranged from 3 to 9 h.

Porous media and impinging jet experiments were performed under comparable near-surface fluid velocities. Comparison of the near-surface fluid velocities between the porous media column and impinging jet systems demonstrates that the fluid velocities used in the impinging jet (1.06 × 10⁻³ and 2.97 × 10⁻³ m s⁻¹) were comparable with 2 and 8 m day⁻¹ in porous media, respectively. Experiments performed in the impinging jet at 2.97 × 10⁻³ m s⁻¹ (16) did not yield ripening; therefore, we performed the additional impinging jet experiments at lower fluid velocities (1.06 × 10⁻³ and 2.12 × 10⁻⁴ m-s⁻¹) to increase the likelihood of observing ripening if it were to occur. Detailed scaling of fluid velocities in two systems was provided in Tong and Johnson (16). Details on the impinging jet system and the corresponding image analysis were provided in a previous publication (15).

Flow Chamber Experiments. Colloid transport experiments were performed in a flow chamber packed with porous media to directly examine colloid deposition. The flow chamber was fabricated from transparent acrylic sheets, with the same dimension as the impinging jet flow cell. Flow chamber experiments were conducted at a pore water velocity of 2 m day⁻¹ at ionic strengths of 0.006, 0.02, and 0.05 M.

The flow chamber was mounted on the microscope stage (Eclipse TE2000-S inverted microscope) (Nikon, Japan). A 10× long-distance working objective (Nikon, Japan) was used to magnify the image. Images were recorded by a CCD camera CoolSNAP HQ (Photometrics, Tucson, AZ) at regular intervals, for example, 10 min, to examine the process of colloid deposition. Photographs were captured using various intensities of both UV and visible headlight at the same time; thus, both fluorescent colloids and glass beads can be simultaneously visualized.

Interaction Force. The Derjaguin, Landau, Verwey, and Overbeek (DLVO) theory was used to calculate the total colloidal interaction force as a function of separation distance. Although other forces may influence the net interaction forces (e.g., hydrophobic, hydration, steric, etc.) (17), we maintain simplicity in this investigation by focusing on van der Waals and electric double layer forces. Colloid−colloid interaction force was determined by treating the colloid−colloid system as a sphere−sphere interaction, whereas colloid−collector interaction force was calculated by treating the colloid−collector system as a sphere−plate interaction.

The retarded van der Waals forces for sphere−sphere and sphere−plate configurations can be calculated by following eqs 1 and 2, respectively (18),

$$F_{vdw} = -\frac{A_{131}a_{p1}a_{p2}}{6h^2(a_{p1}+a_{p2})}\frac{\lambda(\lambda+22.232h)}{(\lambda+11.116h)^2} \quad (1)$$

$$F_{vdw} = -\frac{A_{132}a_p}{6h^2}\frac{\lambda(\lambda+22.232h)}{(\lambda+11.116h)^2} \quad (2)$$

where a_{p1} and a_{p2} in eq 1 refer to the radii of the two interacting spherical colloids, whereas, a_p in eq 2 refers to the radius of

the colloid; h is the separation distance between the two colloids (eq 1) or between colloid and collector surface (eq 2); A_{131} and A_{132} are Hamaker constants for the colloid−water−colloid (4.17×10^{-21} J) and colloid−water−collector (glass) (3.84×10^{-21} J), respectively; λ is the characteristic wavelength of interaction, usually taken as 100 nm.

The electrical double layer forces for sphere−sphere and sphere−plate configurations can be calculated by following equations 3 and 4, respectively (18),

$$F_{EDL} = 4\pi\epsilon_r\epsilon_0\kappa\frac{a_{p1}a_{p2}}{(a_{p1}+a_{p2})}\varsigma_{p1}\varsigma_{p2}\left[\frac{\exp(-\kappa h)}{1+\exp(-\kappa h)} - \frac{(\varsigma_{p1}-\varsigma_{p2})^2}{2\varsigma_{p1}\varsigma_{p2}}\frac{\exp(-2\kappa h)}{1-\exp(-2\kappa h)}\right] \quad (3)$$

$$F_{EDL} = 4\pi\epsilon_r\epsilon_0\kappa a_p\varsigma_p\varsigma_c\left[\frac{\exp(-\kappa h)}{1+\exp(-\kappa h)} - \frac{(\varsigma_p-\varsigma_c)^2}{2\varsigma_p\varsigma_c}\frac{\exp(-2\kappa h)}{1-\exp(-2\kappa h)}\right] \quad (4)$$

$$\kappa = \sqrt{\frac{e^2\sum n_{j0}z_j^2}{\epsilon_0\epsilon_r kT}} \quad (5)$$

where ϵ_0 is the permittivity of vacuum; ϵ_r is the dielectric constant or relative permittivity of water; ς_{p1} and ς_{p2} in eq 3 are the zeta potentials of colloid 1 and 2, respectively, whereas ς_p and ς_c in eq 4 are the zeta potentials of the colloid and the collector, respectively; z_j is the ion valence, e is the electron charge; n_{j0} is the number concentration of ions in the bulk solution. Zeta potentials were calculated from the measured electrophoretic mobilities using the von Smoluchowski equation (19) and were provided in previous publications (15, 16). The von Smoluchowski formula is based on a surface model in which the electric charges are located at the ideal ion-impenetrable surface of zero thickness.

Results and Discussion

The purpose of this work is to examine the transition from conditions under which the colloid breakthrough concentrations during injection were constant (no ripening or blocking) to conditions under which colloid breakthrough concentrations decreased temporally during injection (ripening). To achieve this purpose, experiments were conducted in both packed glass beads and quartz sand columns under identical conditions. No temporal increases in effluent breakthrough concentrations (blocking) were observed under the conditions of the column experiments (Figure 1), due to the low injected concentrations. Injection of high colloid concentrations, for example $>10^{10}$ cells/mL (or injection over long periods) may trigger blocking, as has been observed in many studies (e.g., refs 20, 21).

Temporal constancy of the deposition rate coefficient was observed for all microsphere sizes under conditions of relatively low ionic strength (0.02 M) and relatively high fluid velocity (8 m day^{-1}) (Figure 1, solid square), whereas temporal increase in the deposition rate coefficient (ripening) was observed for all microsphere sizes in response to increased ionic strength and decreased fluid velocity (Figure 1, solid and open triangles). The increase in ionic strength (from 0.02 to 0.05 M) that promoted transition to ripening was small (factor of 2.5), and the decrease in fluid velocity (from 8 m day^{-1} to 2 m day^{-1}) that promoted this transition (at 0.05 M) was also small (factor of 4), indicating that transition from "clean bed" deposition to ripening is possible with relatively subtle changes in solution chemistry and fluid velocity.
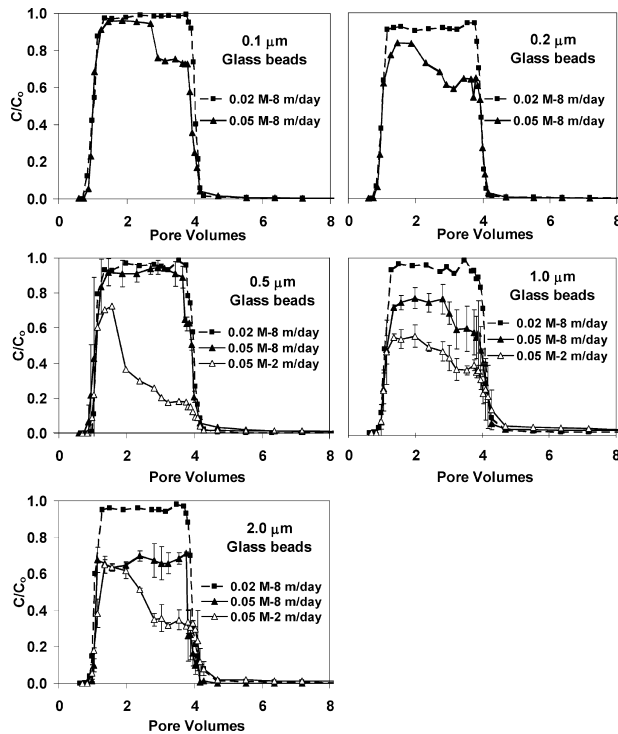
FIGURE 1. Breakthrough curves for different microsphere sizes (0.1−2.0 μm) at fluid velocity = 8 m day^{-1} at an ionic strength of 0.02 M (solid square) and 0.05 M (solid triangle) and at fluid velocity = 2 m day^{-1} at an ionic strength of 0.05 M (open triangle) and pH = 6.72 in glass beads.
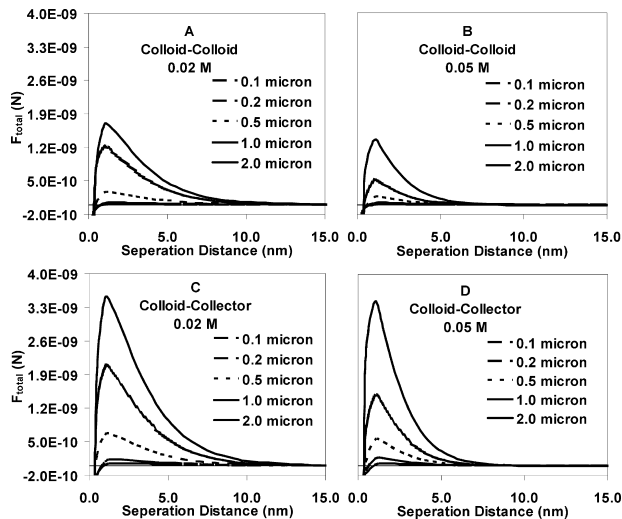
FIGURE 2. Colloid−colloid (above) and colloid−collector (below) interaction force profiles at 0.02 M (left) and 0.05 M (right).

Colloid−colloid and colloid−collector interaction force profiles are shown in Figure 2, and demonstrate that colloid−colloid (Figure 2, panels a and b) and colloid−collector interactions (Figure 2, panels c and d) are repulsive for all microsphere sizes (0.1, 0.2, 0.5, 1.0, and 2.0 μm) under all ionic strengths (0.02 and 0.05 M), with decreases in the interaction energy barriers concomitant with increased ionic strength. Close inspection of the interaction force profiles (Figure 2) demonstrated that colloid−colloid interaction (Figure 2, panels a and b) was somewhat less repulsive than colloid−collector interaction (Figure 2, panels c and d) under all ionic strengths. Furthermore, colloid−colloid interaction was more sensitive to the changes in solution ionic strength relative to colloid−collector interaction, indicating that

increased solution ionic strength favored colloid−colloid interaction relative to colloid−collector interaction.

Direct observation of microsphere (2 μm diameter) deposition was made in a transparent flow chamber packed with porous media under fluid velocity conditions where strong ripening was observed (0.05 M and 2 m day^{-1}). It should be noted that the possible retention of colloids in rear stagnation zones (e.g., ref (22)) was not verifiable using our optical system. Hence, the observations described below concern colloid retention on grain surfaces, for example, grain-to-grain contacts and noncontact areas, and do not address retention in rear flow stagnation zones, although such retention is clearly expected under particular conditions (e.g., ref (23)). After 5 h of colloid injection, images were taken at 70 observation areas constituting the entire area of the entry plane of the flow chamber, to ensure that the observations were representative. Experiments performed at 0.006, 0.02, and 0.05 M were compared and are shown in Figure 3, panels a−c, respectively. At low solution ionic strength (0.006 M), colloid deposition dominantly (~70%) occurred at grain-to-grain contacts (Figure 3a). At intermediate ionic strength (0.02 M), colloid deposition increased (Figure 3b), and colloid deposition occurred at both grain-to-grain contacts (40%) and noncontact areas (60%) (Figure 3b). The decreased dominance of deposition at grain-to-grain contacts with increasing favorability for deposition (increasing solution ionic strength) was in agreement with recent observations for much larger microspheres (36 μm diameter) via X-ray microtomography (24, 25). At an ionic strength of 0.05 M, colloid deposition further increased, and colloid aggregation at grain-to-grain contacts was observed (Figure 3c), in agreement with ripening observed under these conditions (Figure 1). These observations suggest a shift in the dominant mechanism of retention with increased ionic strength (decreased energy barrier height) from single colloid wedging in grain-to-grain contacts to colloid−colloid aggregation in grain-to-grain contacts.

Images of colloid deposition (2 μm diameter, 0.05 M, 2 m day^{-1}) were acquired at 10 min intervals near a randomly chosen grain-to-grain contact (Figure 4). Figure 4, panels a−i, are images of glass beads (gray sphere) and colloids (white) captured at 0, 10, 30, 60, 120, 180, 240, 300, and 360 min of injection, respectively. These results show that significant colloid deposition occurred via interaction with colloids deposited at grain-to-grain contacts. The results presented here indicate that colloid−colloid attachment is facilitated by confinement at grain-to-grain contacts, similarly to wedging that yields colloid deposition between grain surfaces despite the presence of energy barriers between the colloids and the grain surfaces (Figure 2) (23, 25). The confinement between surfaces that yields wedging appears to also facilitate colloid attachment to retained colloids. In other words, the funneling of flow into grain-to-grain contacts allows mobile colloids to overcome repulsion with attached colloids, yielding aggregation.

To contrast the likelihood of colloid−colloid aggregation in grain-to-grain contacts relative to an unbounded surface, experiments were performed under equivalent conditions in an impinging jet system, where the fluid is directed normal to a flat surface and spreads radially. It should be noted that a fluid velocity of 1.06×10^{-3} m s^{-1} was used in the impinging jet system, which yields near-surface tangential fluid velocities that are comparable to those obtained at 2 m day^{-1} in the porous media system (16).

In porous media, the 0.5-μm microspheres showed strong ripening at an ionic strength of 0.05 M and fluid velocity of 2 m day^{-1} (Figure 1), whereas in the impinging jet system, these same microspheres at 0.05 M ionic strength and corresponding fluid velocity (1.06×10^{-3} m s^{-1}) (Figure 5, solid triangle) showed a linear increase in deposited particle
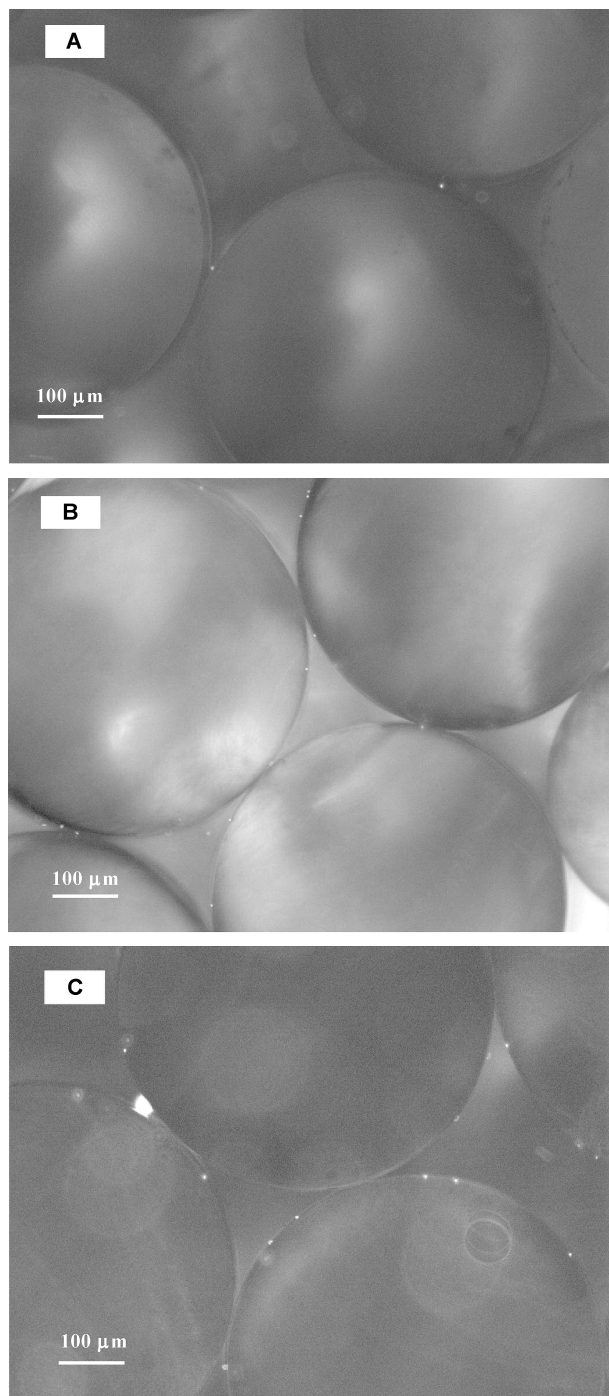
FIGURE 3. Images (magnified 10×) of 2.0 μm microsphere (white spots) deposition in glass beads (gray sphere) at an ionic strength of 0.006 (A), 0.02 (B), and 0.05 M (C) at a fluid velocity of 2 m day^{-1} of injection 5 h in the flow chamber experiments. White flocs (in panel C) are microsphere aggregation.

concentration, indicating a temporally constant deposition flux (no ripening) during the first 6000 min of injection, and lack of colloid−colloid aggregation was also indicated directly in the images. Subsequently, the deposition rate decreased, indicating onset of blocking by previously deposited microspheres. A similar result was obtained at a fluid velocity that was 5 times lower (2.12×10^{-4} m s^{-1}) (Figure 5). The results demonstrate lack of ripening (colloid−colloid aggregation) in the impinging jet system under equivalent conditions that yielded strong ripening in the porous media,
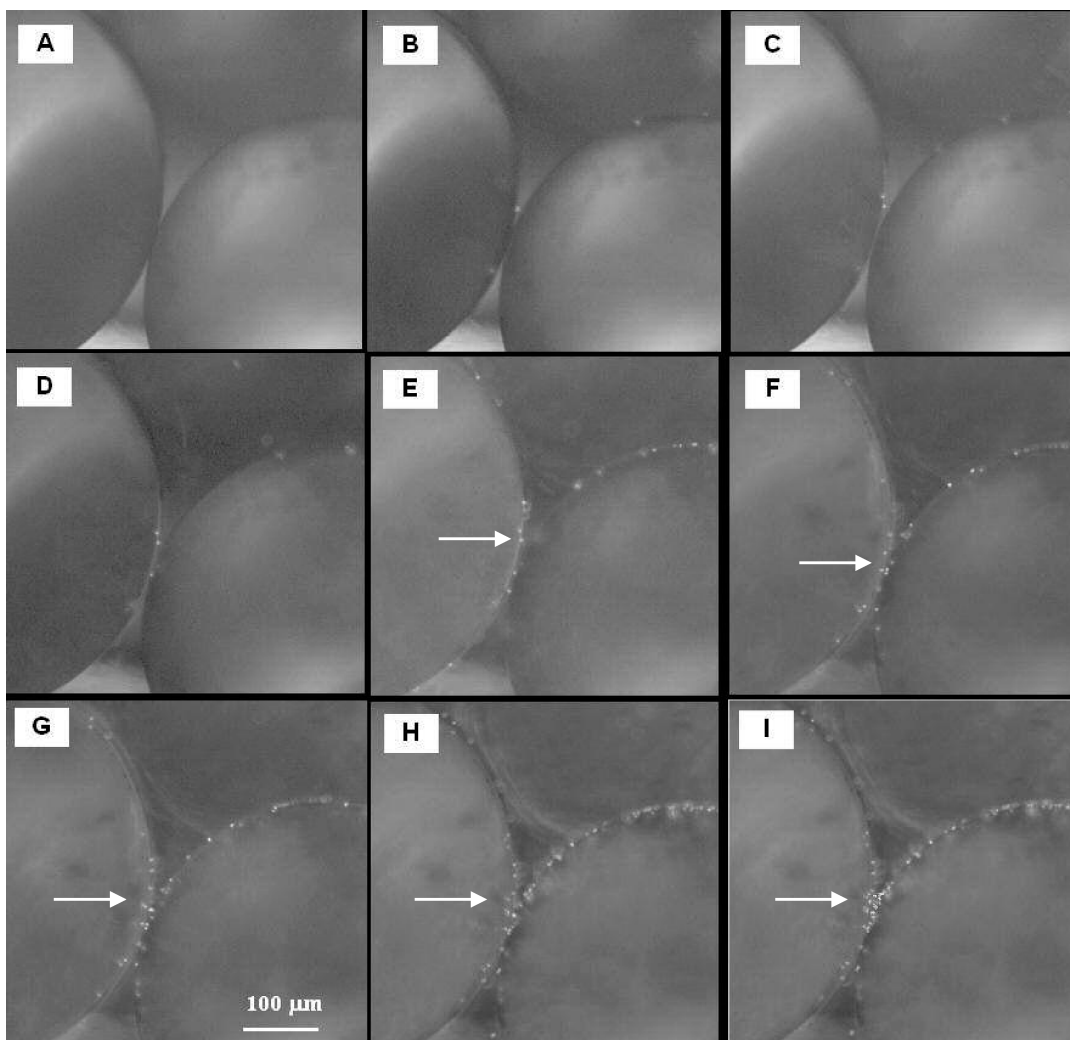
FIGURE 4. Images (magnified 10×) of 2.0 μm microsphere (white spots) deposition in glass beads (gray sphere) captured at different time at an ionic strength of 0.05 M at fluid velocity of 2 m day⁻¹ in the flow chamber experiments. Panels a–i are the images of glass beads (gray sphere) and colloids (white) captured at 0, 10, 30, 60, 120, 180, 240, 300, and 360 min of injection, respectively. White flocs (pointed by an arrow) are microsphere aggregations.
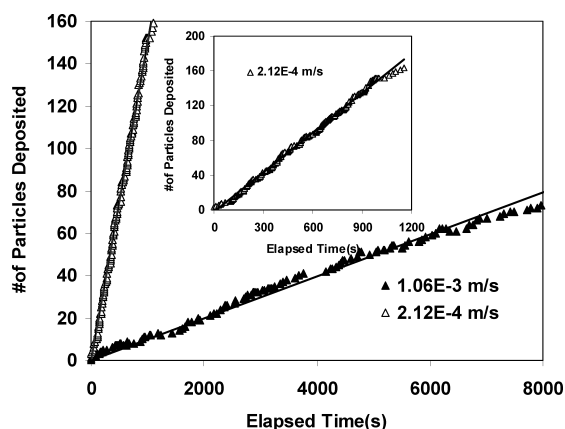
FIGURE 5. Representative net deposition versus time in the impinging jet system for the 0.5 μm microspheres on the glass substratum at fluid velocity of 1.06×10^{-3} m s⁻¹ (solid triangle) and 2.12×10^{-4} (open triangle) at ionic strength = 0.05 M.

indicating that funneling of flow into grain-to-grain contacts contributed to the process of colloid ripening.

Colliding colloids can overcome repulsive colloid–colloid energy barriers as a result of their motion, in a process called "flow-induced aggregation" or "orthokinetic aggregation"

(26, 27). Increased probability of collision between mobile and attached colloids is expected at grain-to-grain contacts relative to noncontact areas due to convergence of flow toward attached colloids at grain-to-grain contacts. Because an excess concentration of mobile colloids occurs in the secondary energy minimum outboard of the energy barrier (23), we can also expect the concentration of mobile colloids to locally increase at the grain-to-grain contact due to convergence of the energy barriers surrounding the two grains. The importance of the colloid–surface energy barrier for promotion of ripening is also indicated by the fact that ripening was observed in the presence of an energy barrier (unfavorable) but not in the absence of an energy barrier (favorable) despite otherwise equivalent conditions (e.g., refs 12, 28).

The extent of colloid wedging in grain-to-grain contacts (direct attachment to porous media) in the presence of an energy barrier was shown to increase with the length and number of grain-to-grain contacts (24, 25) in experiments contrasting deposition in spherical glass beads versus angular quartz sand, with the latter having longer and more grain-to-grain contacts. To examine whether this dependence extends to colloid–colloid aggregation, column experiments were performed in angular porous media (quartz sand with equivalent average size and distribution to glass beads). Figure 6 presents breakthrough curves for five microsphere sizes
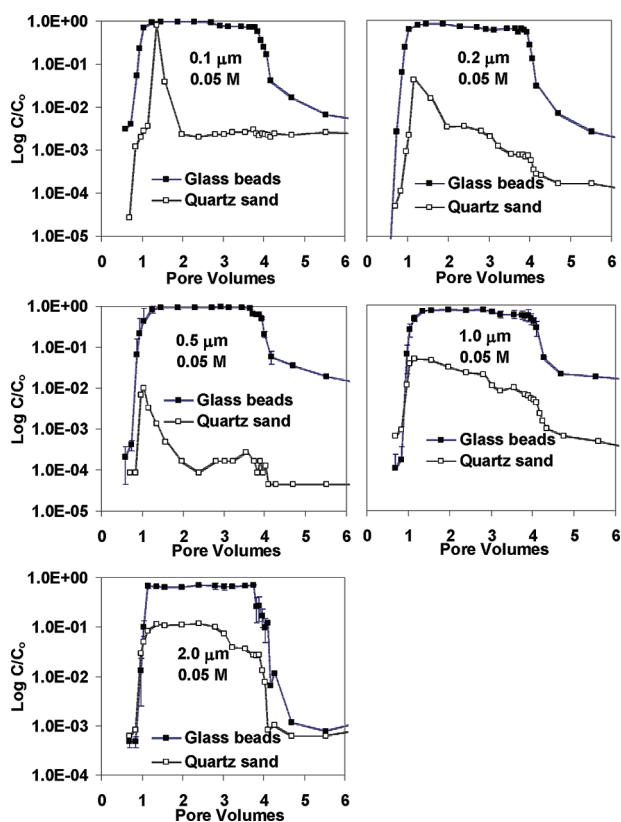
FIGURE 6. Breakthrough curves for different microsphere sizes (0.1–2.0 μm) in quartz sand (open square) compared to glass beads (solid square) at an ionic strength = 0.05 M, pH = 6.72, and at a fluid velocity of 8 m day⁻¹.

(0.1, 0.2, 0.5, 1.0, and 2.0 μm) in quartz sand compared to glass beads at an ionic strength of 0.05 M and a fluid velocity of 8 m day⁻¹. Significant ripening was observed for all microsphere sizes in quartz sand (Figure 6, open square) under these conditions. Moreover, ripening occurred to a much greater extent in quartz sand (Figure 6, open square) relative to glass beads (Figure 6, closed square) during the course of injection. Although it is possible that differences in surface charge heterogeneity of the porous media contributes to the observed differences in retention, we can expect that such heterogeneity would be greater in the glass beads than in the quartz sand. Furthermore, the influence of increased grain-to-grain contact length in the quartz sand was indicated by a previous study (*16*), which demonstrated that colloid retention in quartz sand was twice as high than that in glass beads in the absence of an energy barrier (favorable conditions), where the influence of surface charge heterogeneity was negligible. These observations demonstrated here further implicate that grain-to-grain contacts are important locations for colloid aggregation and indicate that the propensity for colloid aggregation increases with the length and number of grain-to-grain contacts.

Implications. Our results demonstrate that subtle changes in solution chemistry and fluid velocity can trigger transition from "clean bed" deposition to ripening. Furthermore, these results show that ripening involves colloid–colloid aggregation in very specific zones in porous media (grain-to-grain contacts). An important implication of the realization that aggregation occurs dominantly in grain-to-grain contacts is that ripening can be expected to occur at low surface coverage if the surface coverage is calculated from the overall grain surface area. Although surface coverage by attached colloids may be low when considering the overall surface area of the porous media, the accumulation of colloids at grain-to-grain contacts yields high local surface coverage in these zones.

Local high surface coverage by attached colloids at grain-to-grain contacts, combined with the accumulation of mobile colloids in secondary energy minima that merge at grain-to-grain contacts, is expected to yield enhanced probability of collision between mobile and attached colloids at grain-to-grain contacts and is likely to be responsible for the observed aggregation of colloids in these zones.

Literature Cited

(1) O'Melia, C. R.; Ali, W. The role of retained particles in deep bed filtration. *Prog. Wat. Technol.* **1978**, *10* (5–6), 167–182.

(2) Rajagopalan, R.; Chu, R. Q. Dynamics of adsorption of colloidal particles in packed bed. *J. Colloid Interface Sci.* **1982**, *86* (2), 299–317.

(3) Ryde, N.; Kallay, N.; Matijevic, E. Particle adhesion in model systems. Part 14.—Experimental evaluation of multilayer deposition. *J. Chem. Soc., Faraday Trans.* **1991**, *87*, 1377–1381.

(4) Liu, D.; Johnson, P. R.; Elimelech, M. Colloid deposition dynamics in flow through porous media: Role of electrolyte concentration. *Environ. Sci. Technol.* **1995**, *29*, 2963–2973.

(5) Camesano, T. A.; Logan, B. E. Influence of fluid velocity and cell concentration on the transport of motile and non-motile bacteria in porous media. *Environ. Sci. Technol.* **1998**, *32*, 1699–1708.

(6) Camesano, T. A.; Unice, K. M.; Logan, B. E. Blocking and ripening of colloids in porous media: Implications for bacterial transport. *Colloids Surf. A: Physicochem. Eng. Aspects* **1999**, *160*, 291–308.

(7) Tobiason, J. E.; Vigneswaran, B. Evaluation of a modified model for deep bed filtration. *Wat. Res.* **1994**, *28* (2), 335–342.

(8) Tare, V.; Venkobachar, C. New conceptual formulation for predicting filter performance. *Environ. Sci. Technol.* **1985**, *19* (6), 497–499.

(9) Vigneswaran, S.; Tulachan, R. K. Mathematical modeling of transient behavior of deep bed filtration. *Wat. Res.* **1988**, *22*, 1093–1100.

(10) Vigneswaran, S.; Chang, J. S. Mathematical modeling of the entire cycle of deep bed filtration. *Wat. Air Soil Pollut.* **1986**, *29*, 155–164.

(11) Bradford, S. A.; Simunek, J.; Walker, S. L. Transport and straining of E. coli O157:H7 in saturated porous media. *Wat. Resour. Res.* **2006**, *42*,W12S12.

(12) Li, X.; Scheibe, T. D.; Johnson, W. P. Apparent decreases in colloid deposition rate coefficient with distance of transport under unfavorable deposition conditions: a general phenomenon. *Environ. Sci. Technol.* **2004**, *38* (21), 5616–5625.

(13) Tong, M.; Li, X.; Brow, C. N.; Johnson, W. P. Detachment-influenced transport of an adhesion-deficient bacterial strain within water-reactive porous media. *Environ. Sci. Technol.* **2005**, *39* (8), 2500–2508.

(14) Tong, M.; Camesano, T. A.; Johnson, W. P. Spatial variation in deposition rate coefficients under unfavorable deposition conditions resulting from non-electrostatic mechanisms. *Environ. Sci. Technol.* **2005**, *39* (10), 3679–3687.

(15) Johnson, W. P.; Tong, M. Observed and simulated fluid drag effects on colloid deposition in the presence of an energy barrier in an impinging jet system. *Environ. Sci. Technol.* **2006**, *40* (16), 5015–5021.

(16) Tong, M.; Johnson, W. P. Excess colloid retention in porous media as a function of colloid size, fluid velocity, and grain angularity. *Environ. Sci. Technol.* **2006**, *40* (24), 7725–7731.

(17) Ryan, J. N.; Elimelech, M. Colloid mobilization and transport in groundwater. *Colloids Surf. A: Physicochem. Eng. Asp.* **1996**, *107*, 1–56.

(18) Hogg, R.; Healy, T. W.; Fuerstenau, D. W. Mutual coagulation of colloidal dispersions. *Trans. Faraday Soc.* **1966**, *62*, 1638–1651.

(19) Ohshima, H. Electrophoretic mobility of soft particles. *Colloids Surf. A: Physicochem. Eng. Aspects* **1995**, *103*, 249–255.

(20) Adamczyk, Z.; Siwek, B.; Szyk, L. Flow-induced surface blocking effects in adsorption of colloid particles. *J. Colloid Interface Sci.* **1995**, *174*, 130–141.

(21) Bradford, S. A.; Bettahar, M. Concentration dependent colloid transport in saturated porous media. *J. Contam. Hydrol.* **2006**, *82*, 99–117.

(22) Kuznar, Z. A.; Elimelech, M. Direct microscopic observation of particle deposition in porous media: Role of the secondary energy minimum. *Colloids Surf. A: Physicochem. Eng. Aspects* **2007**, *294*, 156–162.

(23) Johnson, W. P.; Li, X.; Yal, G. Colloid retention in porous media: mechanistic confirmation of wedging and retention in zones of flow stagnation. *Environ. Sci. Technol.* **2007**, *41* (4), 1279–1287.

(24) Li, X.; Lin, C. L.; Miller, J.; Johnson, W. P. Pore-scale observation of microsphere deposition at grain-grain contacts over as-semblage-scale porous media domains using X-ray micro-tomography. *Environ. Sci. Technol.* **2006**, *40* (12), 3762–3768.

(25) Li, X.; Lin, C. L.; Miller, J.; Johnson, W. P. Role of grain to grain contacts on profiles of retained colloids in porous media in the presence of an energy barrier to deposition. *Environ. Sci. Technol.* **2006**, *40* (12), 3769–3774.

(26) Elimelech, M.; Gregory, J.; Jia, X.; Williams, R. A. *Particle Deposition and Aggregation: Measurement, Modeling and Simulation*; Butterworth−Heinemann: Oxford, 1995.

(27) Ramachandran, V.; Fogler, H. S. Multilayer deposition of stable colloidal particles during flow within cylindrical pores. *Langmuir* **1998**, *14*, 4435–4444.

(28) Li, X.; Johnson, W. P. Nonmonotonic variations in deposition rate coefficients of microspheres in porous media under unfavorable deposition conditions. *Environ. Sci. Technol.* **2005**, *39* (6), 1658–1665.

ES071888V